JOURNAL OF MATERIALS SCIENCE 21 (1986) 2239–2253

Direct visualization of microstructural deformation processes in polyethylene

W. WADE ADAMS*, D. YANG‡, EDWIN L. THOMAS
Polymer Science and Engineering Department, University of Massachusetts, Amherst, Massachusetts 01003, USA

The deformation morphology of high density polyethylene was investigated by electron microscopy of oriented thin films. A melt-drawing process was used to produce chain axis oriented and planar textured thin film, which was subsequently deformed *in situ* at room temperature in a scanning transmission electron microscope. Both as-drawn and annealed films were studied. Deformation along the orientation direction is initially accomodated by the interlamellar regions, which cavitate and form microfibres. For annealed films it is possible to directly observe strain-induced crystallization at about 300% strain in the fibrils. With increased deformation, suitably oriented lamellar crystals deform by two clearly visualized chain slip systems: {1 0 0}, ⟨0 0 1⟩ and {0 1 0}, ⟨0 0 1⟩. These *c* axis shear processes could be further distinguished as fine slip or as block shear. Still higher deformation causes more breakup of blocks by shear; when the block size is less than some critical size, the blocks decrystallize. The deformation leads toward a fibrillar morphology consisting of oriented crystals from crystallized amorphous material at high elongations, crystal blocks broken out of lamellae, and chains drawn out of lamellae and recrystallized. The deformation behaviour of the as-drawn films is somewhat different from that of the annealed films. Initially as for the annealed films the lamellae are separated with increasing strain as the interlamellar regions are deformed but there is less voiding. Higher deformation causes the lamellae in the as-drawn films to shear apart at significantly lower strain levels (50% as opposed to 300%) than in the annealed films. At about 100% deformation, the as-drawn film no longer has a recognizable lamellar structure. Although generalization is tempered by the simplicity of this model texture, these deformation results are highly relevant to the current microstructural understanding of lamellar deformation in different regions of a spherulite, to the morphology of commercial extruded and blown films, and to specially prepared textured polymers, such as rolled and annealed films or capillary melt flow and solidification methods which can produce texture approaching that of a single crystal.

1. Introduction

Most commercial polymeric products are oriented to some extent. The orientation is either desired (and necessary) as in high strength or high modulus fibres, or is unavoidable, as in injection moulded parts, where the flow of the polymer results in residual orientation even when an isotropic material is desired. The manner in which an oriented polymer deforms is usually quite different from the corresponding isotropic polymer, and the morphology both reflects and controls those differences. Even for a globally isotropic polymer (such as spherulitic polyethylene), the deformation process can be heterogeneous and dependent upon orientation on a small scale, as for example in the different zones of a spherulite. A major problem in the elucidation of the deformation morphology of a semicrystalline polymer is the complexity of the process, primarily due to the hierarchy of structures present. An approach to the determination of the important morphological processes occurring during deformation is the simplification of either the process or the morphology, or both. The study of a model system allows the examination of specific aspects of the deformation process by limiting the complexity of the morphology and hence its response to a specific stress condition.

This paper reports the results of the deformation of such a model system. The production of a near-single crystal texture thin polyethylene film was made possible by modification [1] of Petermann's method [2] for preparation of thin fibre texture film. By using a higher molecular weight polyethylene and melt-drawing from a glass slide at a lower temperature than Petermann, a highly chain axis oriented and planar textured film (uniplanar axial) resulted. This single crystal texture was ideal for *in situ* microscopic deformation studies, which revealed a variety of ultrastructural deformation processes from the application of

**Permanent address*: Materials Laboratory, Wright-Patterson Air Force Base, Ohio 45433, USA.
‡*Permanent address*: Polymer Structure Laboratory, Changchun Institute of Applied Chemistry, People's Republic of China.

0022–2461/86 $03.00 + .12

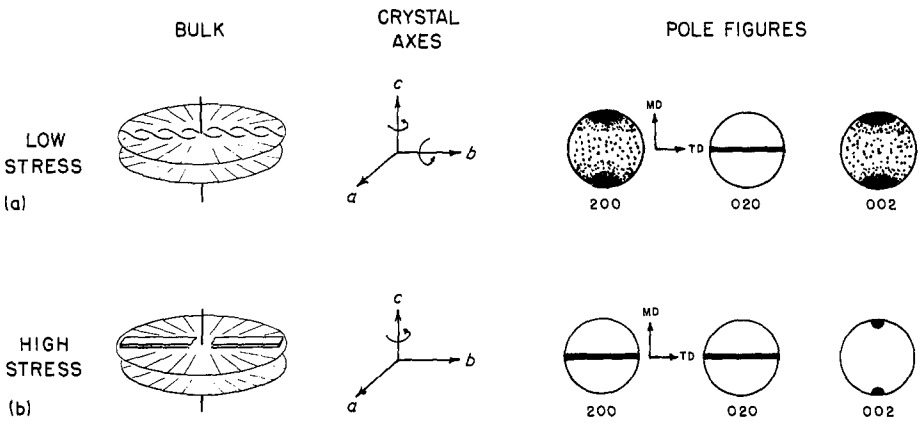

Figure 1 Keller–Machin [35] row structure for uniaxial bulk samples (cylindrites), with ideal pole figures consistent with (a) low and (b) high stress cases (adapted from [10] and [36]).

modern electron microscopic methods [3–5]. These deformation results are relevant to the current microstructural understanding of lamellar deformation in different regions of a spherulite, to the morphology of commercial extruded and blown films, and to specially prepared textured polymers, such as rolled and annealed films or capillary melt flow and solidification methods which can produce texture approaching that of a single crystal. Microstructural deformation processes were clearly imaged in undamaged, unsupported films. Previously these had been inferred from combined X-ray and mechanical tests, or poorly visualized in stained and microtomed samples and in replicas.

2. Background

A common feature in stress-crystallized polymers is the ordered stacking of lamellar crystals perpendicular to the stress direction with fibrillar cores oriented parallel to the stress direction. If most of the chains are extended, then a strong, high modulus fibrous material is the result, as for example, demonstrated by Pennings [6]. More commonly, however, many unextended parts of the chains are available which use the fibres as nuclei for epitaxial crystallization leading to lamellar overgrowths. This is the composite fibre–platelet morphology, or shish-kebab [7].

Orientation induced polymer crystallization historically dates back to rubber network stretching, and the examination of the morphology of stress crystallized rubber has been useful in the understanding of the more modern shish-kebab [8]. The areas of flowing solution induced chain stretching [6], deformation of gel networks [9], and melt drawing [2] have all been very active in recent years, both academically and industrially, since these processes present opportunities for significant advancements in mechanical properties of commonly used polymers. As Keller [7] has pointed out, the deformation of crystalline polymers is also related to the subject of oriented crystallization, since crystallization or recrystallization of oriented chains is operative in the deformation process.

Industrially, production of oriented polymeric materials is very important, and film blowing, extrusion, injection moulding and fibre spinning are probably the most important examples of processes producing large quantities of oriented polymer from the melt [10]. The morphology of the film blowing process has received considerable attention, beginning with the study of hot-extruded low density polyethylene (PE) films by Holmes *et al.* [11] using wide angle X-ray scattering (WAXS). Their conclusions were that the *a* axis of the PE unit cell tended to align along the extrusion direction (MD), and the *c* axis tended to align perpendicular to MD. Keller [12] proposed an alternative morphology, called "row orientation", in which the *b* axis is perpendicular to MD and *a* and *c* have cylindrical symmetry about *b*. The two possible textures could not easily be distinguished by WAXS, and further studies [13] concluded that commercial processes produced textures very much a function of the processing conditions. Lindenmeyer [14] advanced the use of pole figures in texture studies to overcome the limitations of flat film X-ray techniques, and showed that previous studies had been, in fact, inconclusive about the *c* axis orientation. A number of studies have now established the variability of crystallite orientation as a function of process conditions [15–18]. Two distinct types of orientation texture have emerged (Fig. 1), termed high and low stress to reflect their origin. At low elongation rates (low stress), the nuclei (fibrils) are sparsely arrayed, and the lamellar overgrowths can extend far enough to twist, as is also seen for bulk, quiescently crystallized PE. For high rates of elongation (high stress), however, a more dense array of nuclei is produced (fibres), and the lamellar ovegrowths impinge before growing long enough to twist. If the film formation process is constrained to two dimensions, i.e. a very thin film is formed, then it is possible to form a "single crystal" texture, as has been recently demonstrated by Yang and Thomas [1] (see Fig. 2). Bulk samples with single crystal texture have been prepared by various methods, including drawing, rolling and annealing [19, 20]. Such model specimens allowed the first determination of fundamental deformation processes, primarily by combined WAXS and SAXS studies in both extension and compression.

While electron microscopy studies can in principle provide quite detailed microstructural information, the key to any successful investigation is sample preparation. The preparation of thin films which are both suitable for electron microscopy and relevant to understanding some of the details of the deformation processes in semicrystalline polymers is a challenge. Early workers produced thin spherulitic films by quiescent recrystallization of an initial film of polymer

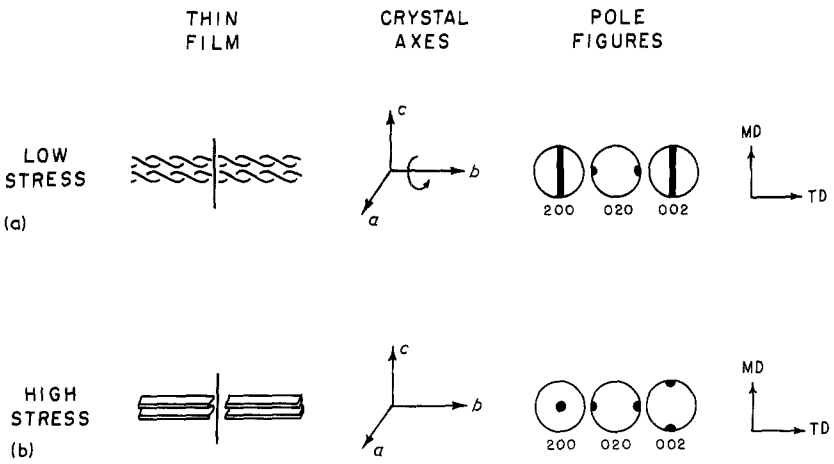

Figure 2 Keller–Machin [35] row structure model for thin films, with ideal pole figures for (a) low and (b) high stress cases (adapted from [10] and [36]).

made thin by solvent casting [21]. Such films when mounted on normal electron microscopy grids could then be deformed by hand permitting interesting although only qualitative observation of the deformation process, which due to the complexity of the film microstructure and uncontrolled mode of deformation was rather difficult to interpret [22].

Petermann [2] found that he could produce well oriented films by drawing a thin film from a molten pool of PE on *o*-phosphoric acid (135 to 200° C). The films produced consist of highly oriented periodic stacks of lamellae exhibiting a fibre texture with their *c* axis along the draw direction. Annealing at high temperatures for long times recrystallized the films with a {1 1 0} surface texture. Fibre symmetry could be restored upon cold drawing. Hot stretching on the other hand produced films with a {2 0 0} surface texture [23]. Deformation studies were conducted by Petermann and co-workers [24, 25] on such melt drawn thin films of various degrees of pre-orientation made possible by varying the melt temperature of the PE from which the film is drawn. Uniaxial deformation at 92° C produced a fibrillar morphology consisting of needle-like, micrometre long crystals for both highly oriented and poorly oriented precursor films. Upon annealing at high temperature the fibrillar material generated by shear deformation of the less oriented precursor film recrystallized into a periodic crystalline/non-crystalline structure whereas the more perfect needle material obtained by unfolding the highly oriented lamellar precursor film was stable with annealing.

In order to produce more highly oriented films, Petermann and Gohil [26] employed melt drawing from a glass surface wherein the better adhesion of the polymer to the glass caused a shorter drawing zone as compared to the phosphoric acid surface (1 μm compared to 1 cm). These films were also found to display fibre symmetry but if formed by drawing just below the melting temperature, a significant (about 1/3) fraction of the material was present in the form of needle crystals in the as-drawn films. Because of these microstructural differences, Petermann's melt drawn films (glass substrate) deform quite differently than *o*-phosphoric acid prepared material [27].

3. Experimental methods

Thin oriented films of high density polyethylene (Marlex 6003 from Phillips Chemical Co., Bartlesville, Oklahoma, $M_w = 2 \times 10^5$, $M_w/M_n = 3$) were prepared by the method of Petermann *et al.* [26], using techniques reported previously [1]. Films drawn from a glass slide at 120° C were used as-drawn (AD) or were annealed on glycerol for 2 h at 128° C (AN). After washing with distilled water, the films were placed upon specially fabricated elongation grids. The electroformed copper grids, manufactured by the Buckbee–Mears Co (St. Paul, Minnesota) were softened by vacuum annealing at 700° C for 18 h. A layer of PE film was placed on the grid, then a region (approximately 2 mm × 0.5 mm) of the film along with the supporting copper wire was removed by cutting with a razor. A second layer of the film was then placed on the grid in the desired orientation for deformation. Adhesion between the layers of PE and between the PE and copper grid allowed the deformation to occur in the unsupported area of gauge length approximately 0.5 mm.

In situ deformation was performed in an elongation sample holder (model SEH) on a JEOL 100CX scanning transmission electron microscope (STEM), operated at 100 kV. Elongations of up to 150 % at room temperature were possible with this method, limited by the catastrophic failure of the unsupported thin polymer film. The deformation rate was 0.05 mm min^{-1}, with an 0.5 mm gauge length, which gives an initial strain rate of 0.1 min^{-1}.

Locally higher deformation was possible by placing a PE film onto a film of evaporated carbon previously placed on the deformation grid in a manner similar to Gohil and Petermann [25]. Deformation of the grid then produced cracks in the carbon perpendicular to the draw direction, over which the polyethylene film was readily drawn to several hundred per cent.

For most conventional transmission electron microscope (CTEM) bright field (BF) photographs, a thin layer of carbon was evaporated onto the deformed thin film in the deformation holder in order to prevent sample motion due to radiation damage while for STEM examinations the carbon was unnecessary. Phase contrast BF images were obtained by defocus of the objective lens [28, 29]. In order to minimize

radiation damage in CTEM, the focusing was carried out on an area, then the sample was translated to an adjacent undamaged area and the image recorded on Kodak SO-163 film using approximately 60% of the crystal lifetime.

STEM techniques were found to be particularly useful, including scanning micro-area electron diffraction [3], and STEM *n*-beam annular dark field (DF) [4, 5]. The high collection efficiency of scattered electrons and selectability of the region imaged were advantageous in observing the *in situ* deformation at successive intervals of increasing strain. For STEM-DF, an area of interest was located at low magnification ($\times$ 10 000 or less), then careful focusing and intensity and contrast adjustment was performed at $\times$ 50 000, using the reduced raster mode to restrict (severe) radiation damage to a small area (typically $\sim 0.5\,\mu m^2$). An image was then recorded on Polaroid Type 55 film at 40 000 instrumental magnification. Optical transforms from CTEM-BF negatives were recorded on Polaroid Type 55 film, using a Polaron optical diffraction system. Spacings due to periodicity in the image were calibrated by a standard of known spacing. Small angle electron scattering (SAES) patterns were recorded using the "high dispersion diffraction" mode on an area selected by the smallest intermediate lens aperture. In this mode, low beam divergence is achieved by use of a small second condenser lens aperture and minimum excitation of the second condenser lens. The intermediate lens and projector lens are adjusted for magnification of the diffraction pattern. The divergence of the incident beam under these conditions was estimated to be 1.5×10^{-5} rad, limiting the maximum resolvable periodic spacing to 250 nm. The camera constant was calibrated by a standard of known spacing (grating replica).

4. Results

4.1. Initial microstructure

The initial microstructure of the thin oriented films was recently reported by Yang and Thomas [1]. Fig. 3 shows a CTEM-BF micrograph of an as-drawn film (designated AD), indicating highly oriented lamellae imaged by defocus phase contrast. The arrow indicates the melt-draw direction, and the electron diffraction pattern Fig. 3c demonstrates that the films consist of oriented crystallites with *c* parallel to the draw direction. The dark patches are crystals that are Bragg-oriented with respect to the incident electron beam. The lamellae are somewhat "wavy" in texture (Fig. 5a), with lengths of 0.2 to 0.5 μm, and with lamellar surface normals of up to $\pm 30°$ to the draw direction. The lamellar thickness (along *c*) is approximately 30 nm and the long period is about 45 nm. The lateral crystal size measures 25 nm (by WAXS and TEM-DF). The AD film has uniplanar texture, with *a* perferentially perpendicular to the film surface, and *b* in the film plane and normal to the draw direction *c* (see Fig. 5a; co-ordinate system shown in Fig. 16).

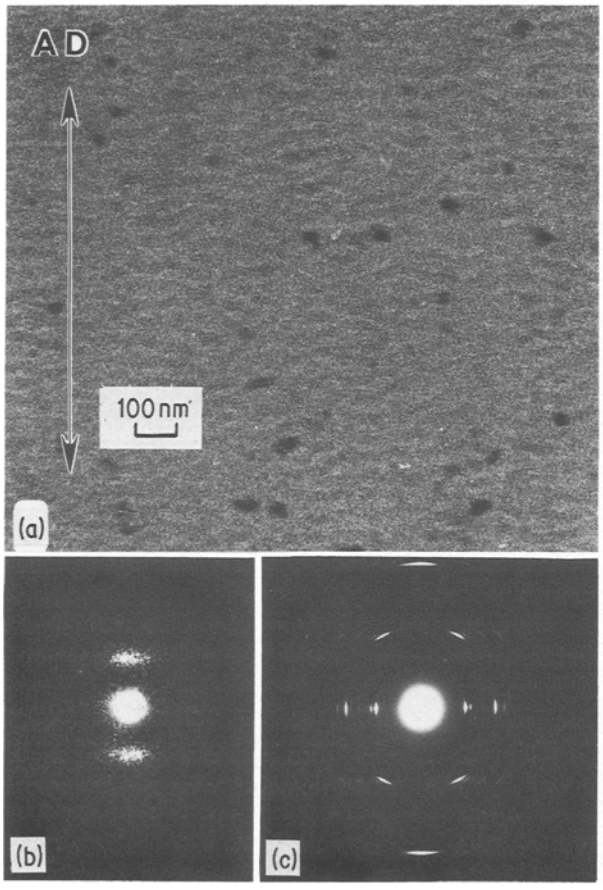

Figure 3 (a) Bright field CTEM micrograph of melt-drawn oriented thin PE film as-drawn (at 120° C), drawing direction vertical (arrow), (b) optical transform of negative and (c) selected area electron diffraction pattern showing high orientation, *c* axis vertical.

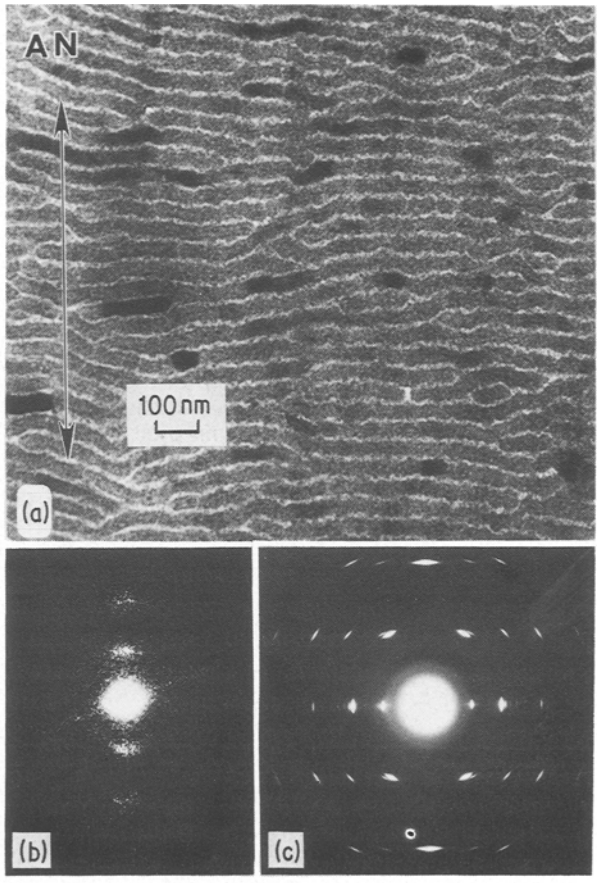

Figure 4 (a) Bright field CTEM micrograph of melt drawn oriented thin PE film annealed for 2 h at 128° C, black regions are Bragg oriented diffracting lamellar crystals, (b) optical transform of negative and (c) selected area electron diffraction pattern showing high orientation *c* axis vertical.

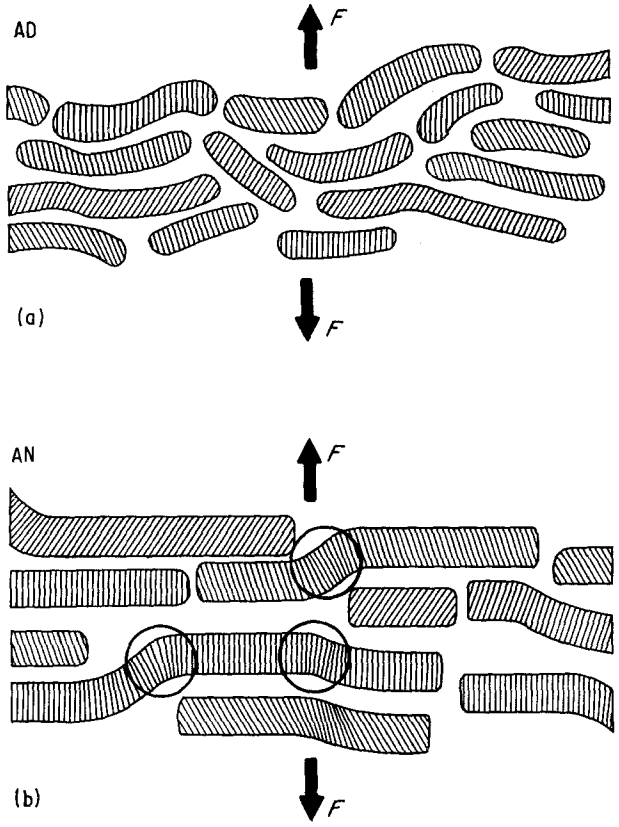

Figure 5 Schematics (a) AD and (b) AN film microstructures.

Upon unconstrained annealing (on the surface of glycerol) at 128° C for 2 h, the film texture does not change, but the *c* axis orientation improves, the long period increases slightly to 48 nm, and the crystal thickness (along *c*) increases significantly to about 37 nm. The lateral crystal size also greatly increases (to nearly 40 nm), and the degree of crystallinity (from differential scanning calorimetry (DSC)) increases from 0.67 to 0.82. After annealing, the lamellae are much straighter and longer (up to 10 μm, see Figs 4 and 5b). The average thickness of the intercrystalline region between adjacent lamellae decreases considerably (from 15 to 11 nm). No extended chain or needle crystals parallel to *c* were observed by electron microscopy or were evidenced by DSC for either AD or AN films.

4.2. Deformation microstructures

Fig. 6 is a CTEM-bright field micrograph of an AN film deformed over a crack in carbon film, deformation direction given by the arrow. The lighter region in the centre is unsupported and has been deformed to approximately 250 % as calculated by measuring the average lamellar spacing and confirmed by optical transforms of the negative. The deformation zone extends into the area supported by the carbon film, and the deformation gradually decreases until, approximately 5 μm from the edge of the carbon film, no deformation is observed. The PE has apparently been pulled away from its close contact with the carbon film. This region of uniformly changing deformation gives rise to a broad maximum along the draw direction (L′) in the small angle electron scattering (SAES) pattern as shown in Fig. 6b. The long period of the undeformed lamellar structure results in the sharp maximum marked L in the schematic (Fig. 6c). The measured SAES long period of 46 nm agrees well with that measured by optical transform (50 nm) and by CTEM-BF (48 nm). The lateral breadth of the long period spot is very narrow,

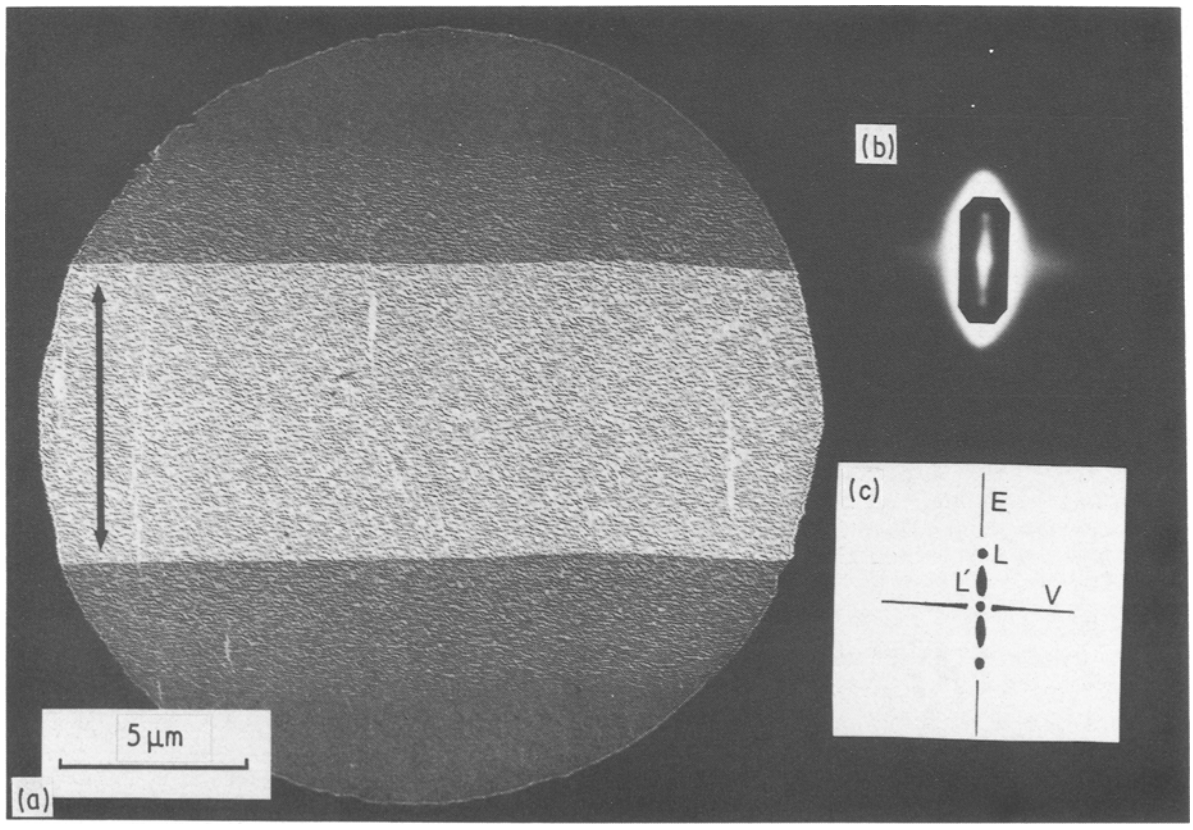

Figure 6 (a) CTEM-bright field micrograph of annealed film deformed over a crack in supporting carbon film, deformation direction vertical (arrow), (b) small angle electron diffraction pattern from this area and (c) schematic of pattern. Letters are explained in the text.

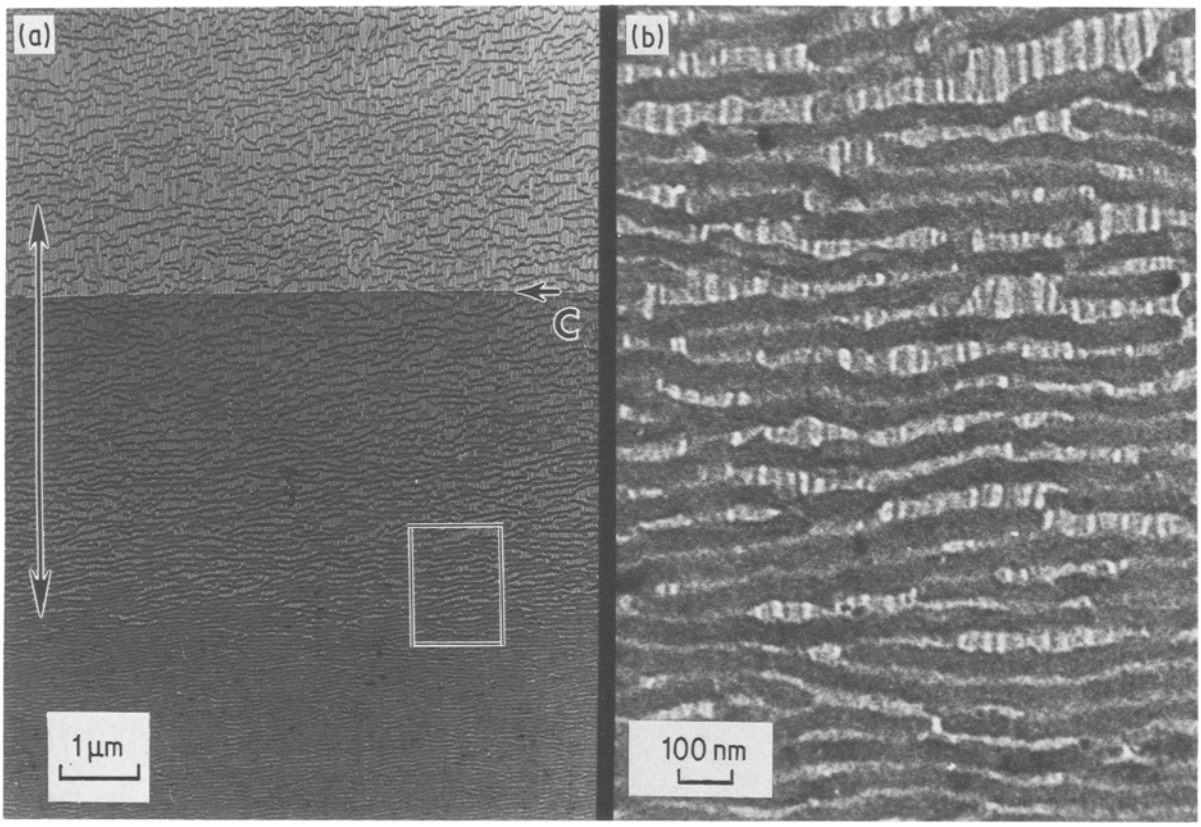

Figure 7 (a) Enlargement of deformed area similar to that of Fig. 6. Carbon film, c, extends vertically to horizontal line marked by short arrow, deformation direction vertical, (b) enlargement of the area outlined by the box. The deformation of the film in this region increases from the bottom of the figure to the top, as one traverses the film towards the unsupported region.

indicating very wide lateral structures (lamellae). The broad maximum L′ due to the deformed region includes spacings from about 55 to 230 nm with a maximum at 900 nm. Other features in the SAES pattern to note include the horizontal streak (V) due to the presence of long, narrow fibres and voids parallel to the stretch direction, and the narrow vertical streak (E) due to scattering from the carbon film edge.

A similar region of this type of deformation is shown enlarged in Fig. 7. The overall deformation mode is more apparent, and consists of separation of lamellae with increasing deformation. The initial deformation occurs entirely in the interlamellar regions, which become thinner and cavitate to form fibres separated by voids (essentially a type of craze). At higher strain levels (toward the top of the images), some regions of the lamellae begin to undergo shear deformation processes. The deformation process will be detailed in the following sections separately for AD and AN films, beginning with the AN films which have considerably clearer deformation microstructures.

4.3. AN films

In Fig. 8 a series of CTEM-bright field micrographs show progressive stages of deformation using the unsupported film deformation method for the 40% deformed sample and the carbon crack method for that with 350% deformation (based on the change from the initial sample long period). The dark regions are Bragg oriented crystals, the white regions oriented parallel to the deformation direction are voids between the darker fibres connecting the separated lamellae. A similar series is shown in Fig. 9 imaged by STEM *n*-beam annular dark field, where diffracting crystals are now white and the voids are black. At small strains, the change in the sample long period is due entirely to deformation in the amorphous zones, which cavitate and fibrillate due to the lateral constraint in the system. This is shown clearly at very high deformation (Fig. 10) where the average long period deformation is 240 %. The crystalline lamellae do not deform until the strain in the amorphous region reaches about 300 %, at which point those regions which have attained the critical resolved shear stress for *c* axis shear begin to slip. In general there are two types of location in the lamellae where crystallographic shear can initiate: (a) regions where the chain axis is misoriented away from the direction of the applied stress (see circled regions in Fig. 5b); and (b) regions where large discontinuities in the tensile loading occur through variations in the local taut tie molecule population along the lamellar surface. Since these films are textured with *c* along the draw direction and *b* predominantly perpendicular to *c* in the plane of the film, *c* axis shear on a plane perpendicular to *b* results in either a continuous "wavy" shear deformation (labelled FS for fine shear in Fig. 12) or a stair–step structure in the lamellae (labelled BS_b for block shear), while shear perpendicular to *a* results in thinner lamellae with mass thickness contrast due to overlapped crystals (labelled BS_a for block shear, also see Figs 11c and d). The intralamellar shear is seen to occur on two different slip systems: {0 1 0}, ⟨0 0 1⟩ and

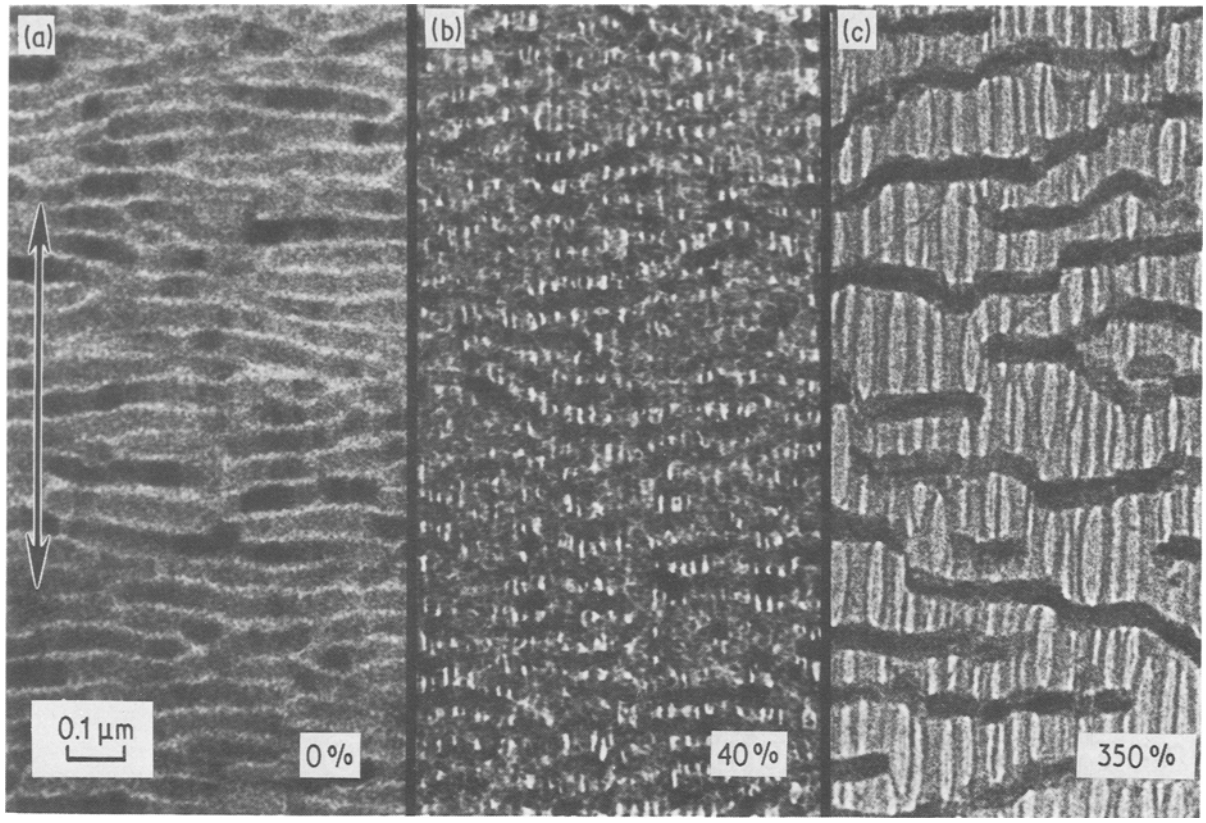

Figure 8 Series of CTEM-bright field micrographs of annealed film at (a) 0%, (b) 40% and (c) 350% elongation as measured by comparing the deformed long period (lamella repeat) to the initial long period.

{1 0 0}, ⟨0 0 1⟩. Other features to note in Figs 11 and 12 are: dark diffracting crystalline regions in the oriented amorphous regions, also seen as white spots in the STEM-DF images; crystals at edges of lamellae in DF images; and fibres apparently extending through (or over/under) lamellae.

Comparison of selected area electron diffraction patterns of undeformed and deformed AN films shows that the *c* axis orientation increases with deformation while the breadth of the equatorial reflections increases, indicating a decrease in the lateral crystal size. A very small amount of the monoclinic crystal form for PE is observed, and the 0 0 2 reflection becomes weaker. A CTEM-dark field image of an

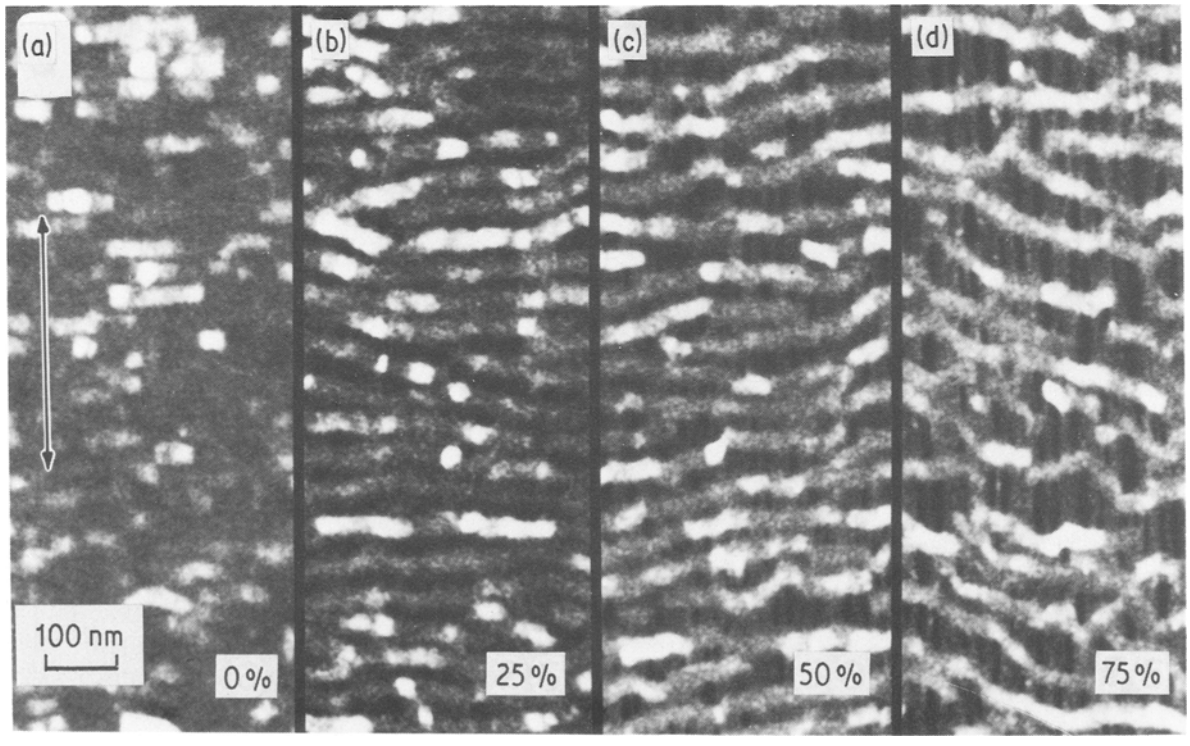

Figure 9 Series of STEM *n*-beam annular dark field micrographs of annealed film: (a) 0%, (b) 25%, (c) 50% and (d) 75% long period deformation, deformation direction vertical.

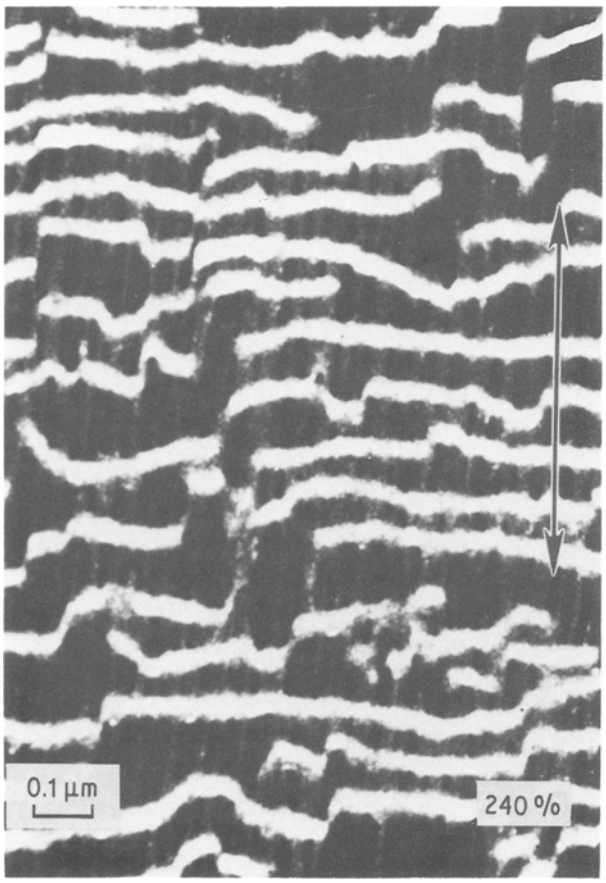

Figure 10 STEM *n*-beam annular dark field micrograph of annealed film, 240% long period deformation, deformation direction vertical.

annealed film deformed to 300 % is shown in Fig. 13. The large white areas are lamellar crystals, but now at this deformation small crystals in many of the fibres are visible. Some of the crystals in the fibres are long and narrow, but most are more nearly equiaxial approximately 6 nm in size; a few fibres show a periodic arrangement of crystals along the fibre axis.

4.4. AD films

Fig. 14 shows a series of CTEM-BF micrographs for the AD films at successive stages of deformation. The distinction of crystalline lamellae in the images is much more difficult due to the smaller crystal size and perfection. The deformation behaviour is somewhat different to that of the AN films: initially as with the the AN films, the lamellae are separated with increasing strain as the intercrystalline region is stretched, but there are fewer voids found in the AD case, and they are smaller. Further deformation causes the AD crystalline lamellae to break up at significantly lower strain levels (50% as opposed to 300%) than do the AN crystalline lamellae, mostly by $\{0\,1\,0\}$, $\langle 0\,0\,1\rangle$ slip. The ease of crystal shear is apparent in Fig. 15 as the large bright crystals, easily seen in the STEM-DF image at 0%, nearly all disappear into the mottled background at modest ($\sim 50\%$) deformation compared to the AN films. At about 100% deformation, the film no longer has any recognizable lamellar structure.

5. Discussion

5.1. "Amorphous" fibres

When the oriented lamellar films are deformed along the MD the deformation initially occurs entirely in the intercrystalline regions. The amorphous polymer between two adjoining lamellae behaves as a compliant rubber, becoming thinner in the normal direction (ND) and trying to become thinner in the transverse direction (TD) as it is lengthened along the MD. This is depicted in Fig. 16, where the initial deformation results in a thinner "film" between lamellae (Fig. 16b), which can be seen in the low deformation areas in Fig. 7. For the AN films, the lateral stress on the non-crystalline region becomes large enough at high stretch to cause cavitation and the interlamellar region resembles a craze (Fig. 16c). The AD films with their inherently more defective and misoriented lamellae undergo a more homogeneous deformation without the formation of distinct craze-like structures in the interlamellar regions. The amorphous fibres in the AN films differ in lateral size, probably due to different local levels of stress and film thickness. At a strain of about 300 to 350% (in the interlamellar region) the entangled non-crystalline chains have reached their elongational limit, which for HDPE has been estimated to be 370% [30]. More elongation would require bond breakage or a higher temperature to give the chains enough mobility to disentangle. Since the thicker, more perfect and better aligned crystalline lamellae in the AN films resist plastic deformation to higher levels of applied strain, the elongated "amorphous" fibres in the AN films strain crystallize. The crystal size is small (5 to 15 nm), limited both by the lateral size of the fibres and the very high undercooling (room temperature deformation). These fibrillar crystals can best be seen as white spots in the CTEM-dark field image in Fig. 13, examples marked by the small arrows distinguish them from the large residual lamellar crystals (large arrow). A periodic arrangement of these crystals in the fibre direction is occasionally seen.

The appearance of the AN films at low deformation is superficially similar to that of the "hard elastic" fibres (see [31] for a brief review), where small voids are opened by a (reversible) cavitation and elastic lamellar bending. The low deformation voiding process in our films was observed to be qualitatively reversible upon relaxation of the applied stress, but a quantitative study remains to be performed. Cayrol and Petermann [32] in their early studies also noted the resemblance to the "hard elastic" materials.

5.2. Deformation of lamellae

The annealed films deform along the MD in a manner much like that depicted by Schultz [33] and Fig. 17 is a modification of his version of Peterlin's deformation model. At high strain some crystallization occurs in the extended non-crystalline fibres (see Fig. 17a) resulting in strain hardening such that the lamellar crystals begin to deform. As previously discussed, they can deform in several ways. The lowest energy response is *c* axis slip [34]. Figs 17b and c show both "block" slip and fine slip due to either the resolved shear stress reaching a critical value or due to an

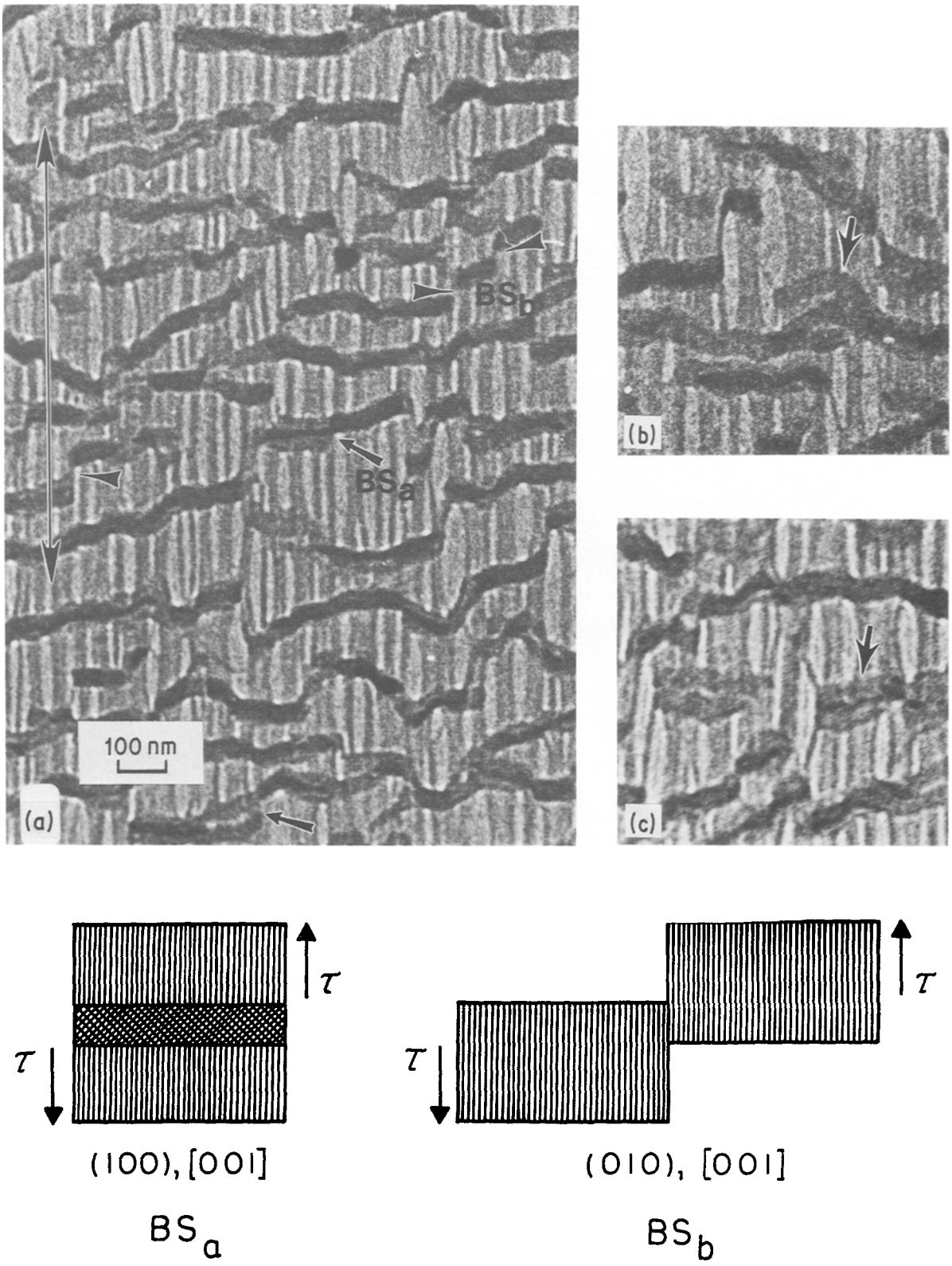

Figure 11 (a) CTEM-bright field micrographs of deformed AN films. BS_a and BS_b refer to lamellae deformed by block shear. (b) Lamellae (arrow) sheared by combined block shear (1 0 0) and fine shear (0 1 0), (c) lamellae (arrow) having undergone block shear (1 0 0) producing overlapping lamellae and (d) schematics of observed block shear processes.

imbalance in the local tensile loading leading ultimately to a fibre structure. To Schultz's summary of the deformation process we can add two new items (marked * and † below) [33]:

First stage: lamellae move rigidly apart with strain accommodated almost entirely by the interlamellar amorphous layer.

Second stage: tie chains become highly extended and slip initiates in the crystalline lamellae.

*Strain induced crystallization of the oriented amorphous fibres occurs.

Third stage: blocks of crystal are pulled out of the lamellae.

†As block shear continues, portions of lamellae which are below a critical size (for the particular T_{draw}) decrystallize and contribute to strain softening.

Fourth stage: both the blocks from crystal shear processes and strain induced crystallization become aligned along the tensile axis.

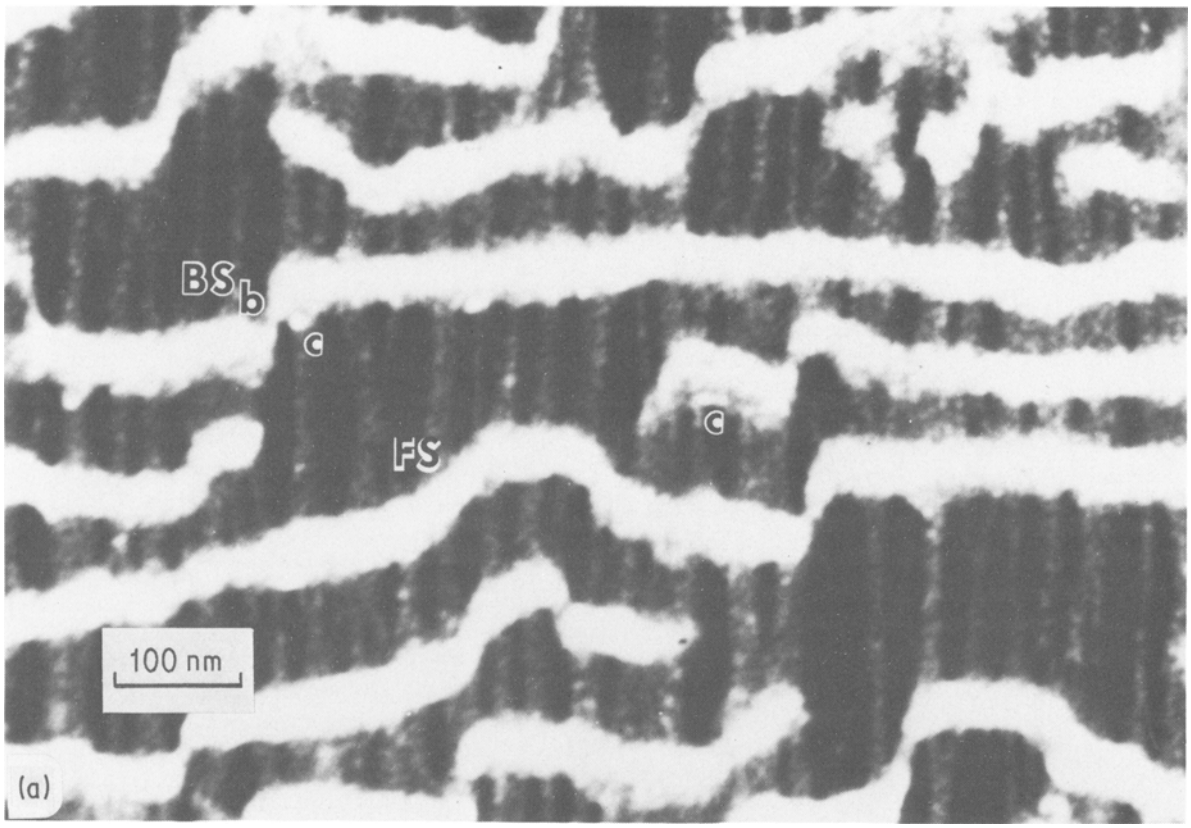

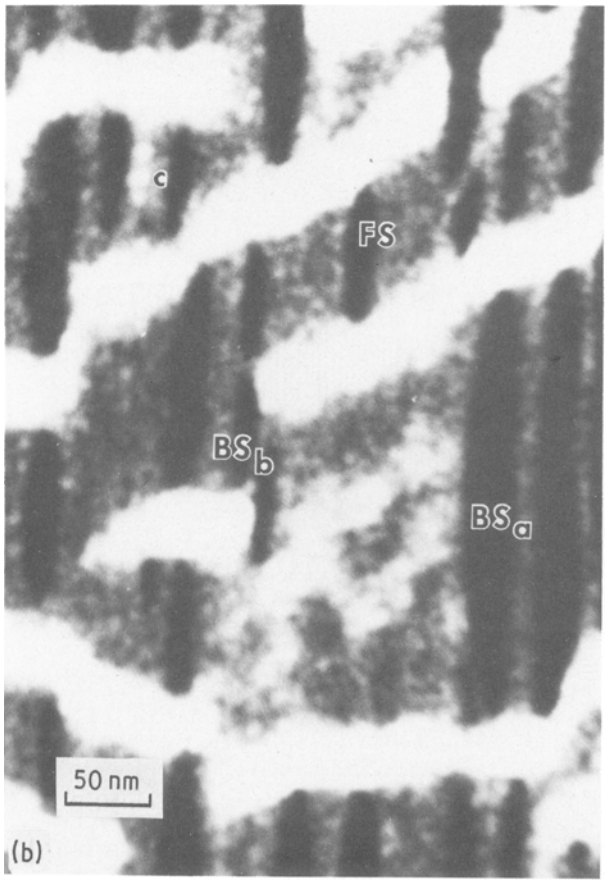

Figure 12 (a) and (b) STEM-DF images of deformed AN films showing fine shear (FS), block shear (BS) and many strain induced crystals in fibre areas (labelled c).

The shear processes of the crystalline lamellae have been inferred mostly from combined X-ray and mechanical property studies, and Bowden and Young [34] have summarized the processes. On a molecular level, Fig. 18 gives the basis for distinguishing the fineness of slip. Fig. 18a is uniform fine slip, where every two chains are displaced one lattice vector along *c*. Coarser slip (referred to here as block slip) is shown in Fig. 18b, with blocks of chains (4 shown) slipping by 2 lattice vectors to give the same total shear deformation as Fig. 18a.

Block slip can be further distinguished by the plane of shear as either (1 0 0) or (0 1 0). This difference is modelled in Figs 11d and 19 where (1 0 0), *c* axis slip is seen in Fig. 19b, and (0 1 0), *c* axis slip is shown in Fig. 19c. Combinations are also possible, depicted in Fig. 19d to produce successively smaller blocks. The actual slip systems are indeed recognizable in these highly textured films, as shown in Fig. 12. Block slip is labelled BS with a subscript for the plane on which the shear operates. Fine shear is seen many places, and is labelled as FS. CTEM-BF images give exceptional detail for these slip systems, and Fig. 11 gives examples of all 3 types of slip. Figs 11b and c show two regions demonstrating these features. For example, (1 0 0), *c* axis shear (BS_a) is manifested by an increase in the BF image intensity in the regions of the lamellae that are displaced and no longer overlap. In other words, the dark band in the centre of the lamellae (parallel to *b*) is indicative of the original thickness (along *a*) of the lamellar crystal, and the lighter grey areas are thinner portions of the crystal translated apart by shear (Figs 11c and d).

With increasing deformation, the sheared lamellae can break up further by more slip, and/or folded chains can be directly pulled out. As the process continues to the point at which the crystal block size is less

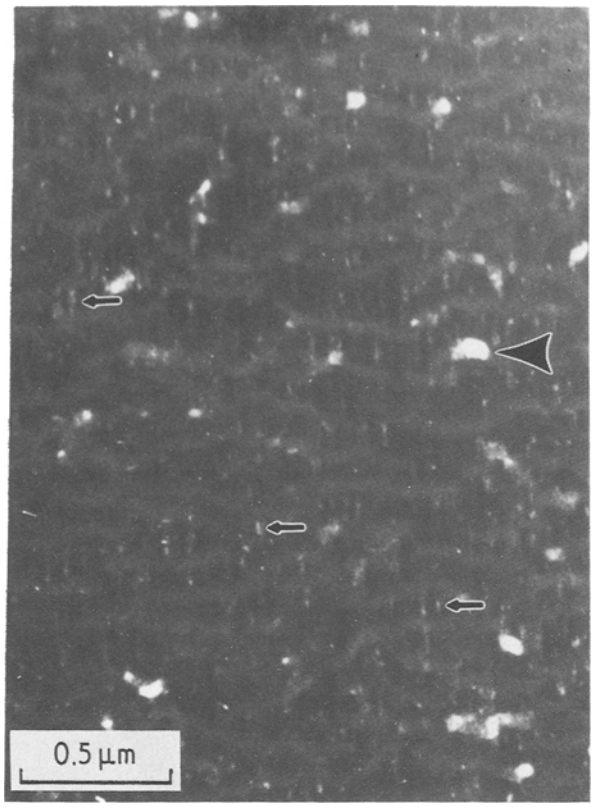

Figure 13 CTEM-dark field image using the 1 1 0, 2 0 0 reflections of an AN film deformed to 300% strain. Large arrow points to a lamellar crystal and the small arrows indicate small crystals in the highly strained amorphous regions.

than a critical size for the particular drawing temperature, the block decrystallizes contributing to strain softening, concomitantly strain hardening occurs with recrystallization of the highly drawn chains in the fibre structure.

6. Conclusions

The study of the morphology of the deformation process for bulk spherulitic polymers is a challenge, complicated by the hierarchical morphology. The approach used in this paper involved the study of a model system that allowed simplification of both the morphology and the deformation process. This simplification of the problem enabled the examination and elucidation of specific ultrastructural deformation processes which had heretofore only been partially inferred by indirect measurement or poorly visualized in previous microscopy studies.

The systems studied were near-single crystal texture thin polyethylene film made by modification of Petermann's method. Samples were melt-drawn from a glass slide at 120° C to give highly chain axis oriented and planar textured film (*a* perpendicular to the plane of the film; *b* perpendicular to *c* and in the plane of the film, parallel to the long dimension of the well formed lamellae). Films were examined both in their as-made state (AD) and after high temperature annealing (AN). The films were deformed *in situ* at room temperature in a scanning transmission electron microscope.

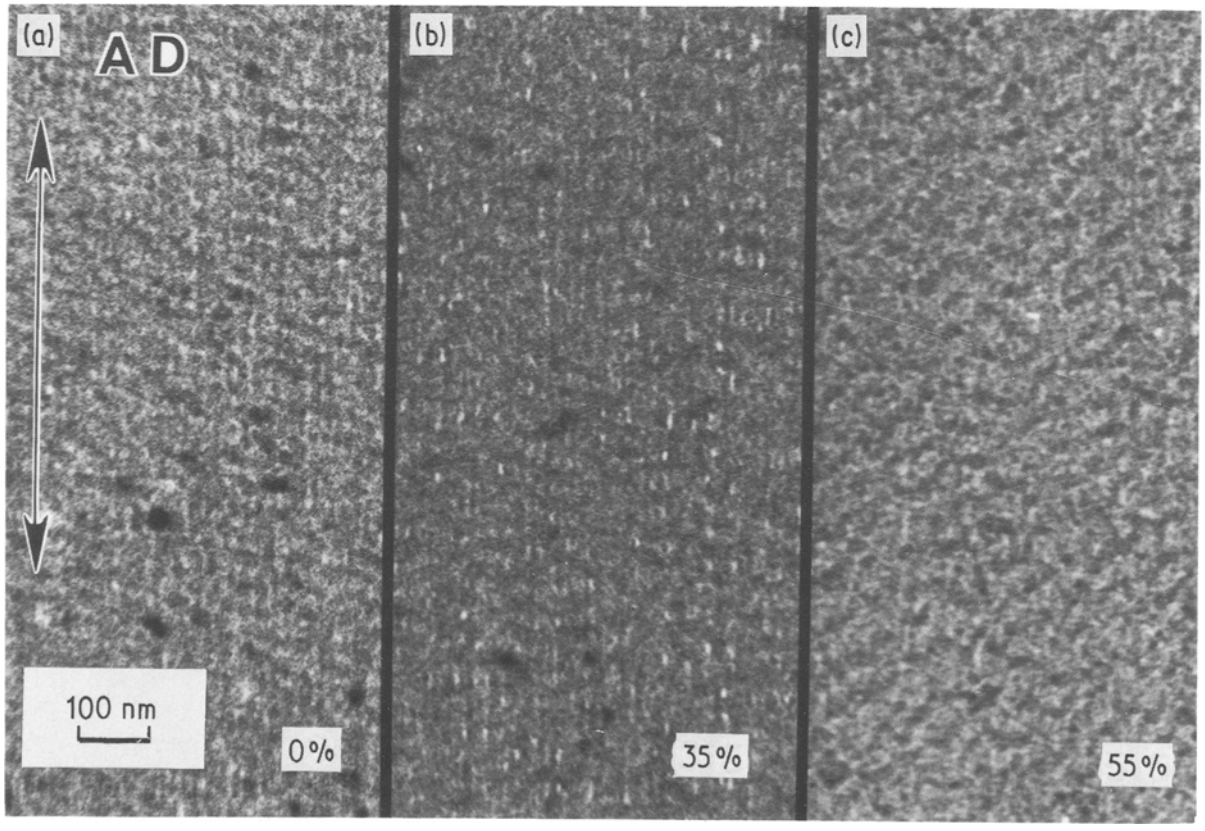

Figure 14 CTEM-bright field micrograph series of as-drawn film (deformation vertical) at (a) 0%, (b) 35% and (c) 55% long period strain.

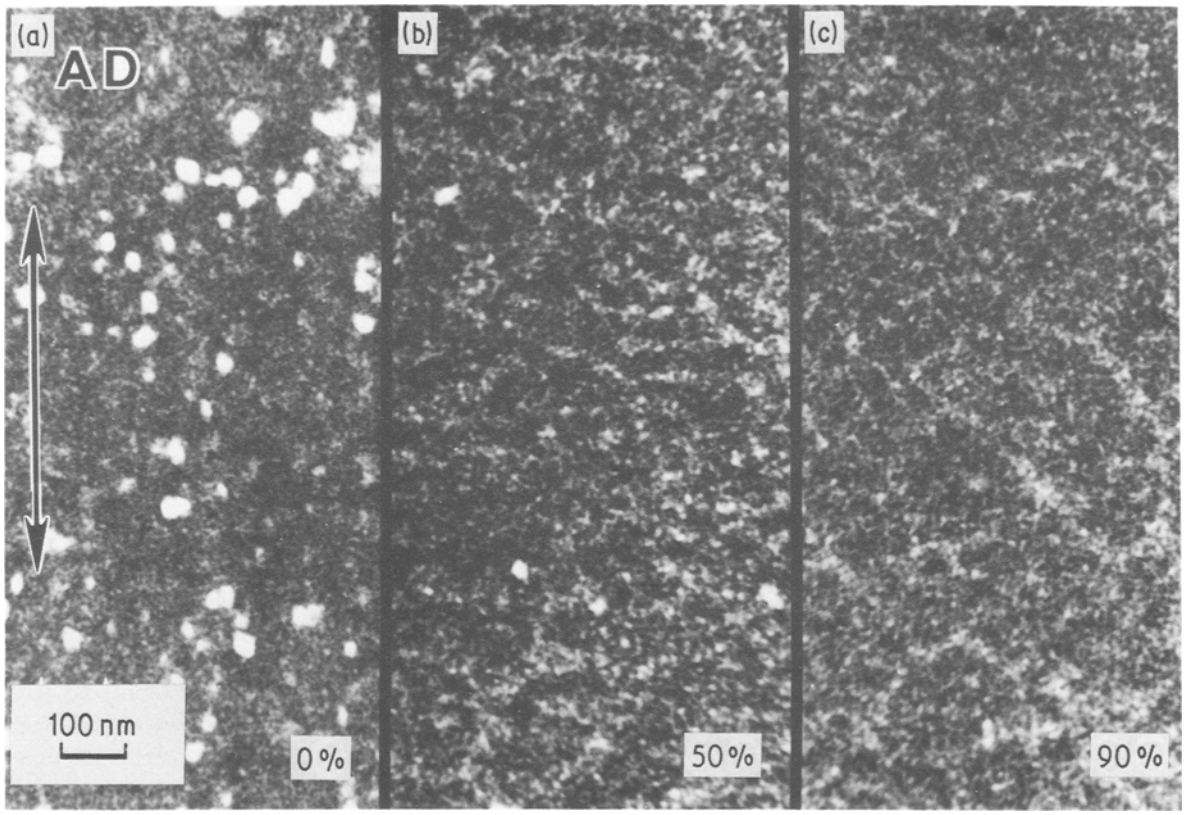

Figure 15 STEM *n*-beam annular dark field image series of as-drawn film, deformation vertical, at (a) 0%, (b) 50% and (c) 90% long period strain.

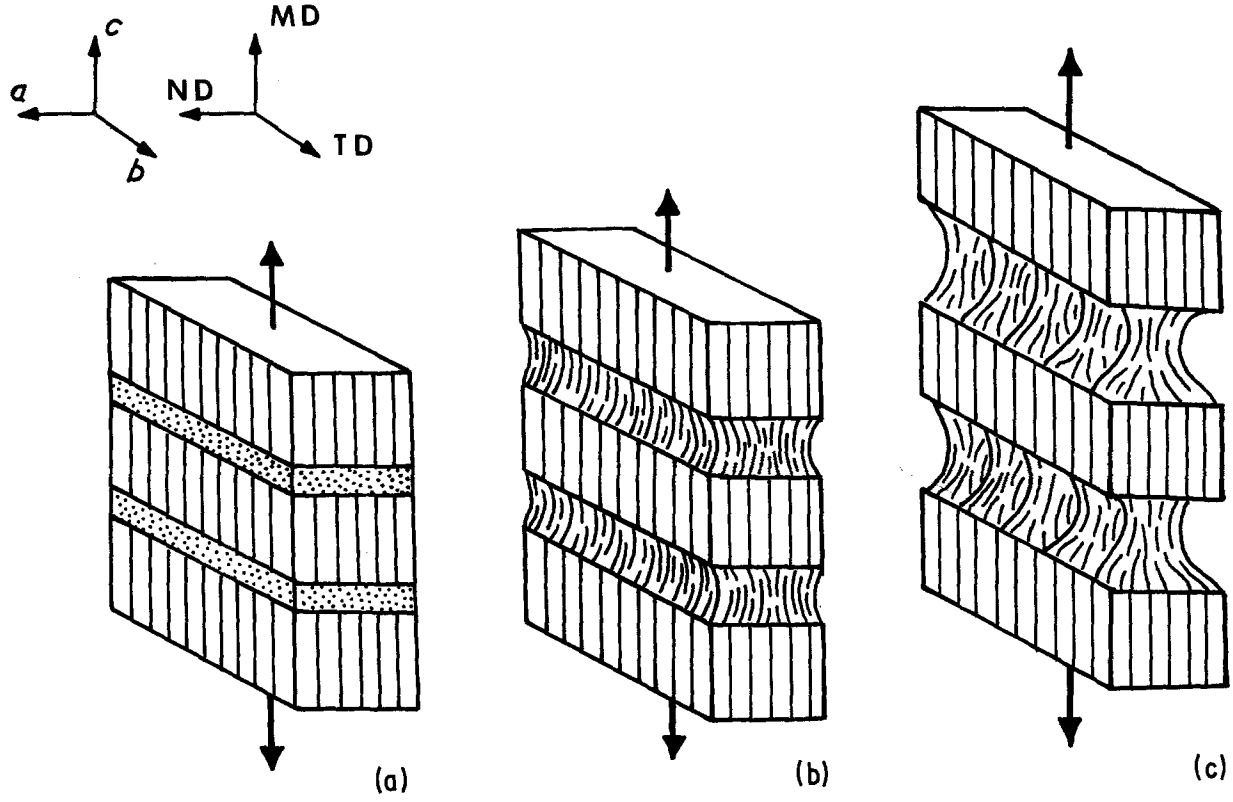

Figure 16 Schematic showing the elongation of the rubber-like amorphous zones into fibres with increasing strain (a) 0%, (b) 100% amorphous strain, 20% long period strain, (c) 400% amorphous strain, 60% long period strain. Co-ordinate systems are indicated for crystal axes and for film directions: MD is machine direction, TD transverse direction and ND normal direction.

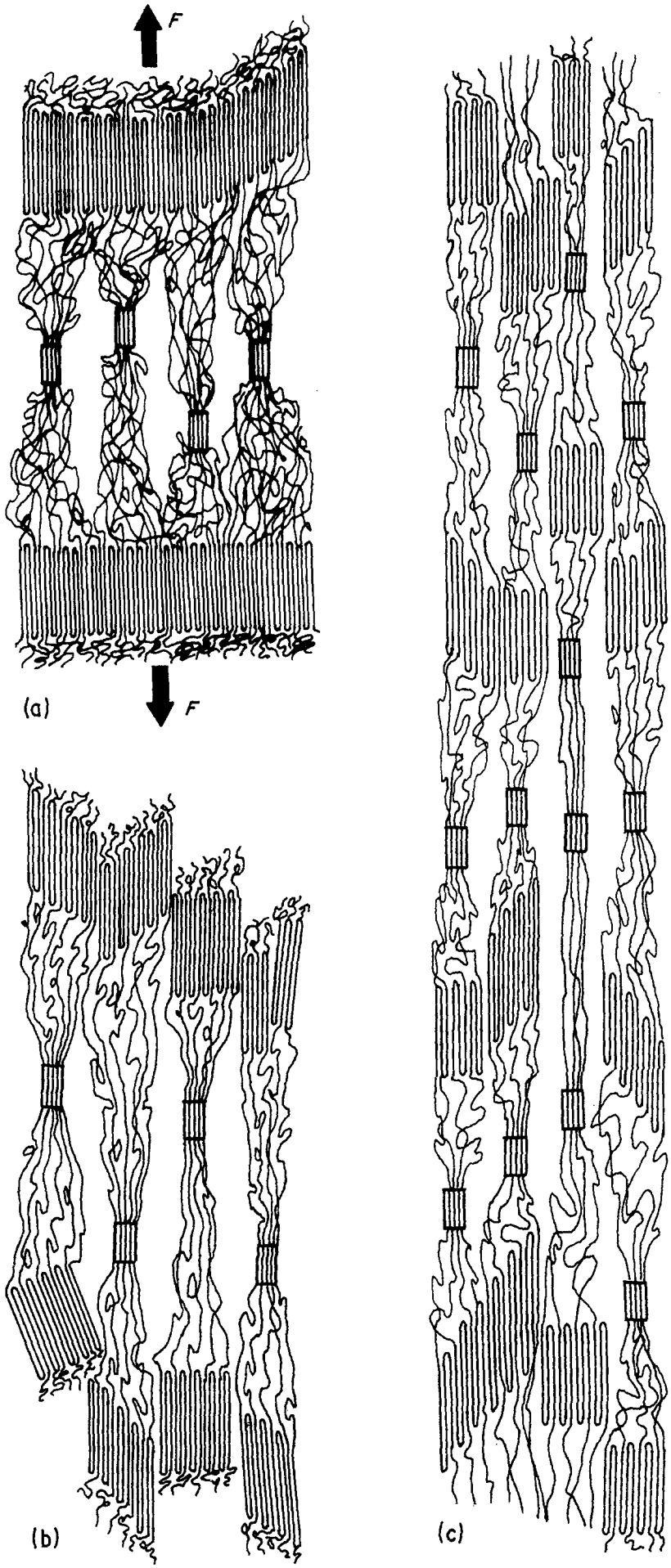

Figure 17 Drawing after Schultz [33] of the ultrastructure of deformation, (a) strain in amorphous regions sufficient to induce crystallization in the fibres, (b) block slip resulting in breakup of lamellae into large blocks and (c) fibrillar morphology with discrete microfibres containing some lamellar block crystals and strain induced fibrillar crystals.

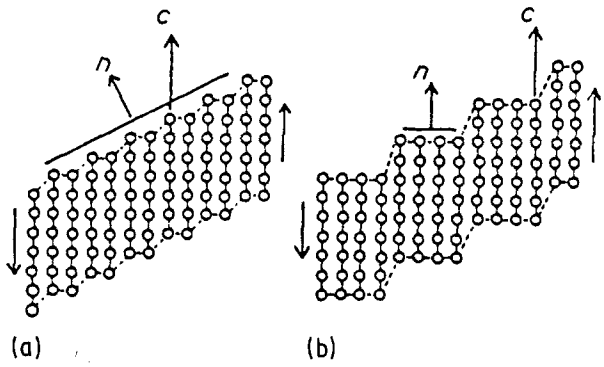

Figure 18 Schematic diagrams taken from Young and Bowden [37] illustrating different degrees of fineness of slip. (a) Fine slip. A displacement of one lattice vector has occurred on every other lattice plane in the crystal. The direction n is the normal to the surface of the crystal which has rotated relative to the chain axis c during deformation. (b) Coarse slip. The same total shear has been produced by a displacement of two lattice vectors on every fourth plane.

For the AN films, deformation along the orientation direction at low strain is accomodated entirely by the interlamellar regions, which cavitate to form fibrils due to lateral constraint. At strains of about 300 % in the fibrils, strain induced crystallization was observed in the AN films, which contributes to strain hardening of the system. With further deformation, the lamellar crystals deform by chain slip processes. Two slip systems were clearly visualized: {1 0 0}, ⟨0 0 1⟩ and {0 1 0}, ⟨0 0 1⟩. The c axis shear process was further resolved into fine slip due to small continuous chain slip increments on (0 1 0) planes, or block slip where large blocks shear on either the (1 0 0) or (0 1 0) or both planes. Still higher deformation causes more breakup of blocks by shear, with some pullout of folded chains. When the sheared block size becomes less than some critical size, the block decrystallizes, which contributes to strain softening. Thus, in these films melting is seen to be a natural result of

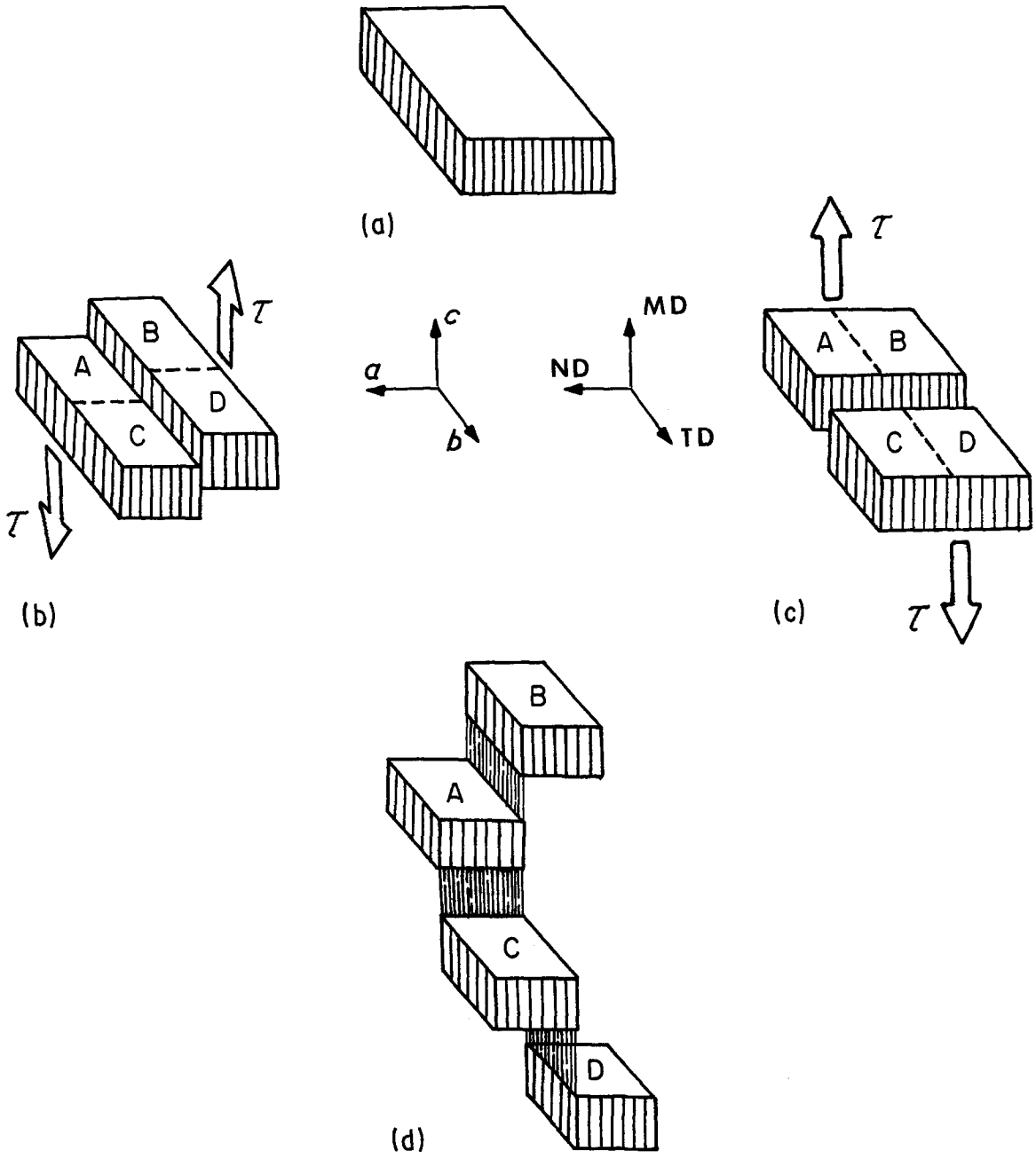

Figure 19 Schematic drawing of the block slip mechanisms, (a) undeformed lamellar block, (b) (1 0 0), ⟨0 0 1⟩ slip producing long, thin sheared lamellae, (c) alternatively, (0 1 0), ⟨0 0 1⟩ slip producing stair step sheared lamellae and (d) combined shear modes leading to reduction of block size.

crystal shear processes while, at the same time, recrystallization in the drawn fibrils occurs. Both the blocks from crystal shear and strain induced crystallization become aligned along the tensile axis.

The deformation behaviour of the AD films is somewhat different than that of the AN films. Initially as for the AN films the lamellae are separated with increasing strain as the interlamellar regions are deformed but there is less voiding. Higher deformation causes the lamellae in the AD films to shear apart at significantly lower strain levels (50% as opposed to 300%) than in the AN films. At about 100% deformation, the AD film no longer has a recognizable lamellar structure.

Acknowledgement

Financial support was received from NSF through Grants DMR 80-12724 and DMR 84-06079 (Polymer Division). The use of the University of Massachusetts MRL facilities is appreciated.

References

1. D. YANG and E. L. THOMAS, *J. Mater. Sci.* **19** (1984) 2098.
2. J. PETERMANN and H. GLEITER, *Phil. Mag.* **28** (1973) 1279.
3. E. S. SHERMAN and E. L. THOMAS, *J. Mater. Sci.* **14** (1979) 1109.
4. E. S. SHERMAN, W. W. ADAMS and E. L. THOMAS, *ibid.* **16** (1981) 1.
5. V. P. CHACKO, W. W. ADAMS and E. L. THOMAS, *ibid.* **18** (1983) 1999.
6. A. J. PENNINGS, *J. Polym. Sci. Symp.* **59** (1977) 55.
7. A. KELLER, *Proc. R. Soc., Faraday Disc.* **68** (1979) 145.
8. E. H. ANDREWS, *Int. J. Polym. Mater.* **2** (1973) 337.
9. P. SMITH and P. J. LEMSTRA, *J. Mater. Sci.* **15** (1980) 505.
10. E. S. CLARK and C. A. GARBER, *Int. J. Polym. Mater.* **1** (1971) 31.
11. D. R. HOLMES, R. P. PALMER, R. G. MILLER and C. W. BUNN, *Nature* **171** (1953) 1104.
12. A. KELLER, *J. Polym. Sci.* **15** (1955) 15.
13. D. R. HOLMES and R. P. PALMER, *ibid.* **31** (1958) 345.
14. P. H. LINDENMEYER and S. LUSTIG, *J. Appl. Polym. Sci.* **9** (1965) 227.
15. C. R. DESPER, *ibid.* **13** (1969) 169.
16. W. F. MADDAMS and J. E. PREEDY, *ibid.* **22** (1978) 2721.
17. *Idem, ibid.* **22** (1978) 2739.
18. *Idem, ibid.* **22** (1978) 2751.
19. A. KELLER and D. P. POPE, *J. Mater. Sci.* **6** (1971) 453.
20. D. P. POPE and A. KELLER, *J. Polym. Sci. (Phys.)* **13** (1975) 533.
21. H. D. KEITH and F. J. PADDEN Jr, *J. Polym. Sci.* **41** (1959) 525.
22. I. L. HAY and A. KELLER, *Kolloid-Z.Z. Polym.* **204** (1965) 43.
23. B. CAYROL, J. KUBAT and J. PETERMANN, *Makromol. Chemie* **175** (1974) 3557.
24. J. PETERMANN, W. KLUGE and H. GLEITER, *J. Polym. Sci. (Phys.)* **17** (1979) 1043.
25. R. M. GOHIL and J. PETERMANN, *ibid.* **17** (1979) 525.
26. J. PETERMANN and R. M. GOHIL, *J. Mater. Sci.* **14** (1979) 2260.
27. J. PETERMANN, R. M. GOHIL, M. MASSUD and D. GORITZ, *ibid.* **17** (1982) 100.
28. J. PETERMANN and H. GLEITER, *Phil. Mag.* **31** (1975) 929.
29. M. J. MILES and J. PETERMANN, *J. Macromol. Sci. (Phys.)* **B16** (1979) 243.
30. D. T. GRUBB, *J. Polym. Sci. (Phys.)* **21** (1983) 165.
31. A. PETERLIN, *Polym. Eng. Sci.* **16** (1976) 126.
32. B. CAYROL and J. PETERMANN, *J. Polym. Sci. (Phys.)* **12** (1974) 2169.
33. J. SCHULTZ, in "Polymer Materials Science", (Prentice Hall, New Jersey, 1974) p. 499.
34. P. B. BOWDEN and R. J. YOUNG, *J. Mater. Sci.* **9** (1974) 2034.
35. A. KELLER and M. J. MACHIN, *J. Macromol. Sci. (Phys.)* **B1** (1967) 41.
36. T. NAGASAWA, T. MATSUMURA and S. HOSHINO, *Appl. Polym. Symp.* **20** (1973) 295.
37. R. J. YOUNG and P. B. BOWDEN, *J. Mater. Sci.* **8** (1973) 1177.

Received 11 June
and accepted 10 July 1985